

## Using experimental data to test an $n$ -body dynamical model coupled with an energy-based clusterization algorithm at low incident energies

Rohit Kumar and Rajeev K. Puri\*

*Department of Physics, Panjab University, Chandigarh - 160014, India*

(Received 27 February 2018; published 30 March 2018)

Employing the quantum molecular dynamics (QMD) approach for nucleus-nucleus collisions, we test the predictive power of the energy-based clusterization algorithm, i.e., the simulating annealing clusterization algorithm (SACA), to describe the experimental data of charge distribution and various event-by-event correlations among fragments. The calculations are constrained into the Fermi-energy domain and/or mildly excited nuclear matter. Our detailed study spans over different system masses, and system-mass asymmetries of colliding partners show the importance of the energy-based clusterization algorithm for understanding multifragmentation. The present calculations are also compared with the other available calculations, which use one-body models, statistical models, and/or hybrid models.

DOI: [10.1103/PhysRevC.97.034624](https://doi.org/10.1103/PhysRevC.97.034624)

### I. INTRODUCTION

It is well accepted that multifragmentation plays decisive role in understanding reaction dynamics [1–12]. The theoretical description of this phenomena is debated equally by two types of models: (i) statistical models (based on the assumption of thermal equilibrium) and (ii) dynamical models (capable of following reaction dynamics from the start to the end). The main disadvantage of statistical models such as the microcanonical multifragmentation model (MMM) [13], the statistical multifragmentation model (SMM), [14], etc. is that they completely disregard reaction dynamics and, moreover, one has to start the calculations assuming some initial conditions (such as temperature, excitation energy, freeze-out volume, fragmenting-source size, etc.) either parametrized or obtained from some experimental determinations [13,14]. On the other hand, dynamical models have the advantage of following the reaction dynamics from the start to the end where matter is fragmented. These models include numerically different solutions of the time evolution of the one-body or  $n$ -body dynamics [8–12,15,16]. The understanding of the fragment formation is considered to be well governed by the  $n$ -body models because of the perseverance of event-by-event correlations among nucleons.

A typical transport model generates a phase space of nucleons only, so one has to use a clusterization algorithm to identify multibound fragments. In the literature, several attempts have been reported in this direction [12,17–22]. In one of the first attempts, fragments were identified on the basis of spatial correlations among nucleons at the fag end of the collisions [12]. This algorithm was dubbed the “minimum spanning tree” (MST) method and is found to explain experimental results only for limited entrance channels [22,23]. Therefore, various improvements were also proposed

to obtain realistic fragments such as introducing additional momentum constraints among nucleons, restructuring fragments, or subjecting each fragment to fulfill binding-energy constraints, etc. [18–22]. These methods helps in improving the consistency of calculations with experimental results, but only for the central reactions. The failure of the QMD + MST model (to explain experimental results) also raised questions about the reliability of the QMD model to describe the density fluctuations and excitation energies for mildly excited nuclear matter [5]. Based on these results, the need for statistical decay codes such as SMM and GEMINI was also felt [14,24]. On the other hand, contrary to the above results, Muller *et al.* [25] showed that the decay properties of excited nuclei are well reproduced in the  $n$ -body QMD model.

Another question regards the timescale of the formation of fragments. The noble clusterization algorithm called the “early cluster recognition algorithm” (ECRA) [26] based on the simulated annealing technique was introduced in this regard. It showed the early formation of clusters. Based on the same annealing method, the simulated annealing clusterization algorithm (SACA) [27] and the fragment recognition in general application (FRIGA) [28] were later put forward. The consistency of QMD + SACA method with experimental results scraps many gray areas of QMD model (or in general for models based on the  $n$ -body theories), proposed on the basis of results obtained by using the MST method as fragment identifier [29,30]. To add to this, even the timescale of the fragment realization has been significantly improved compared with MST or its variants. Note that, in all these studies [29,30], only average observables with limited entrance channels were used. To get in-depth knowledge of the dynamics of reactions, one also has to investigate more complex observables.

With the advancement of the technology, it has become possible to accurately detect the charged as well as uncharged particles. As a result, more exclusive and complex observables have been constructed. In this regard, Rivet *et al.* [31] and Frankland *et al.* [6] put forward one of the complete sets

\*drkpuri@gmail.com

of experimental data for the reactions of  $^{129}\text{Xe} + ^{119}\text{Sn}$  and  $^{155}\text{Gd} + ^{238}\text{U}$  at incident energies of 32 and 36 MeV/nucleon, respectively. They mainly reported the charge distribution of fragments, *the event-by-event distribution of the three largest charges*, multiplicity distribution of fragments, and the bound-charge distribution within each event. Both Rivet *et al.* [31] and Frankland *et al.* [6] tried to reproduce these results by using one-body models, the stochastic initialization method (SIM), and Brownian one-body dynamics (BOB) calculations coupled with the statistical decay code SIMON [32].

On the other hand, Raduta *et al.* [33] employed MMM calculations with two fragment-formation conditions [13,33] and deexcitation code at later times of the reaction [34]. In MMM calculations, a complete equilibrium hypothesis was considered whereas, in the case of SIM and BOB calculations, collisions were first done by using BNV equations with a stochastic force term added to calculations at the time when the system enters the spinodal region and continuously, respectively. The equilibrium hypothesis was applied at later times,  $\sim 200$  fm/c, followed by statistical decay codes to deexcite the fragments [32].

A careful analysis of literature shows that the reactions  $^{40}\text{Ca} + ^{40}\text{Ca}$  [35] and  $^{197}\text{Au} + ^{197}\text{Au}$  [7] were also performed at the same excitation energies, where charge distribution and event-by-event *distribution of the first six largest charges* (for  $^{197}\text{Au} + ^{197}\text{Au}$  reaction) were reported. To confront the experimental results of  $^{40}\text{Ca} + ^{40}\text{Ca}$  [35] reactions, initial conditions were followed by using BNV and BUU calculations and injected into several statistical models of Sa and Gross [36], Richert and Wagner [37], and GEMINI [24]. The results of  $^{197}\text{Au} + ^{197}\text{Au}$  were confronted with the statistical multifragmentation model with two-model source conditions [7].

Interestingly, to best of our knowledge, no  $n$ -body dynamical model such as the QMD model was ever robust against these experimental results. At the same time, as we see from above, the multitude of models were needed to explain experimental data partially or full. In the present paper, we plan to see the compatibility of the QMD model coupled with the SACA method to describe the observables that check the event-by-event correlations among fragments and to judge whether applying a multitude of theoretical models for a single experimental result is indeed needed or it is just failure of the statistical or dynamical models for not being able to describe experimental data by using an individual model. The choice of these experimental observables is made by keeping in mind the following:

- (1) Although the mass and asymmetry varies drastically in these reactions, their corresponding excitation energy is same in all these reactions.
- (2) The availability of theoretical calculations of one-body dynamical models [6,31], statistical models [7,13,33,34], and/or hybrid models (where dynamical models are coupled with statistical models) [24,35–37] gives us a unique opportunity to do comparative analysis.

This paper is structured as follows: Sec. II gives a very brief information of our primary model QMD and clusterization

algorithm SACA. A detailed comparison of our calculations and the above-mentioned experimental data together with other model predictions is presented in Sec. III. Conclusions are drawn in Sec. IV.

## II. THE MODEL

### A. Quantum molecular dynamics model

The quantum molecular dynamics (QMD) model [12] is a classical many-body theory in which some quantum features due to the fermionic nature of nucleons are also included. The QMD model simulates the reactions and generates the phase-space of nucleons on an event-by-event basis. Here each nucleon in the colliding system is represented by a Gaussian in momentum and coordinate space as

$$\psi_i(\vec{r}, \vec{p}_i(t), \vec{r}_i(t)) = \frac{1}{(2\pi L)^{\frac{3}{2}}} e^{[i\vec{p}_i(t)\cdot\vec{r} - \frac{|\vec{r}-\vec{r}_i(t)|^2}{4L}]}. \quad (1)$$

Mean position  $\vec{r}_i(t)$  and momentum  $\vec{p}_i(t)$  are the two time-dependent parameters. The centroids of these Gaussian wave packets propagate in coordinate and momentum space according to classical equations of motion:

$$\dot{\vec{r}}_i = \frac{\partial H}{\partial \vec{p}_i}, \quad \dot{\vec{p}}_i = -\frac{\partial H}{\partial \vec{r}_i}, \quad (2)$$

where  $H$  is the total Hamiltonian of the nucleon consisting of Skyrme, Yukawa, and Coulomb interactions. We basically follow the framework of Ref. [12]. For details of the model, we refer the reader to our previous works [19,22,27,29,30]. Since in the QMD model, the time evolution of collisions is done at the nucleonic level, therefore, it is necessary to transform nucleonic information into fragment information by means of fragment-recognition algorithm. We used SACA as the fragment identifier in the present study.

### B. Simulated annealing clusterization algorithm

This noble algorithm is based on the principle of energy minimization of fragmenting system and allows the fast realization of fragment structures [27]. According to this algorithm, a group of nucleons are part of a bound fragment if their total binding energy per nucleon  $\zeta_i$  is less than a certain value:

$$\zeta_i = \sum_{i=1}^{A_f} \left[ \sqrt{(\vec{p}_i - \vec{p}_{A_f}^{\text{c.m.}})^2 + m_i^2} - m_i + \frac{1}{2} \sum_{j \neq i}^{A_f} V_{ij}(\vec{r}_i, \vec{r}_j) \right] < E_{\text{Bind}} A_f, \quad (3)$$

with  $E_{\text{Bind}} = -4.0$  MeV if  $A_f \geq 3$  and  $E_{\text{Bind}} = 0.0$  otherwise. In the above equation,  $A_f$  is the number of nucleons in fragment and  $\vec{p}_{A_f}^{\text{c.m.}}$  is the center-of-mass momentum of that fragment. The purpose of implementing a binding-energy check is to reject the unbound fragments which will decay at later times. The details of the algorithm are given in Ref. [27].

## III. RESULTS AND DISCUSSIONS

For the present analysis, thousands of events were simulated for the reactions of  $^{40}\text{Ca} + ^{40}\text{Ca}$ ,  $^{129}\text{Xe} + ^{119}\text{Sn}$ ,  $^{155}\text{Gd} + ^{238}\text{U}$ , and  $^{197}\text{Au} + ^{197}\text{Au}$  at incident energies of 35, 32, 36, and

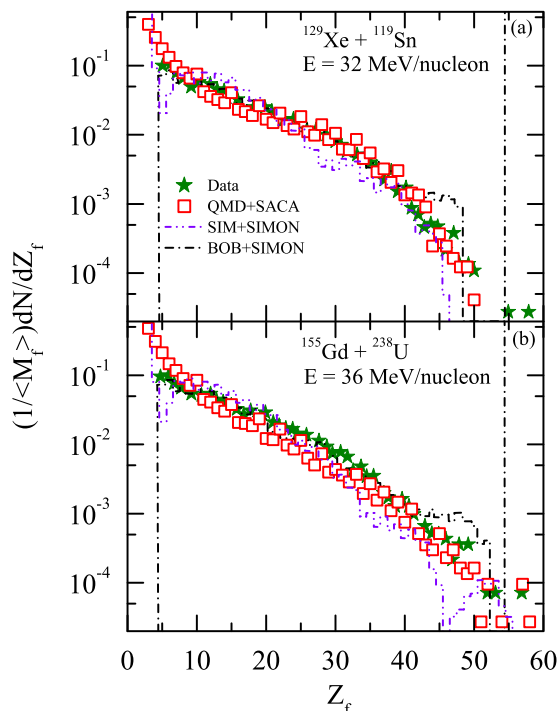


FIG. 1. The normalized charge distribution obtained in the central reactions of  $^{129}\text{Xe} + ^{119}\text{Sn}$  and  $^{155}\text{Gd} + ^{238}\text{U}$  at an incident energy of 32 and 36 MeV/nucleon, respectively. The stars represent experimental data [6] and squares represent the calculations of QMD coupled with SACA algorithm. The results of previous attempts [6,31] are also displayed for comparison.

35 MeV/nucleon, respectively. The soft equation of state along with energy-dependant nucleon-nucleon cross section was employed. The phase space of nucleons was then injected into SACA to obtain fragment information.

In Fig. 1, we display the normalized charge distribution obtained in the central reactions of  $^{129}\text{Xe} + ^{119}\text{Sn}$  and  $^{155}\text{Gd} + ^{238}\text{U}$  at incident energies of 32 and 36 MeV/nucleon, respectively. In these reactions, the system mass varies from 248 to 393 units, whereas the excitation energy per nucleon of the composite system formed during the reaction is almost constant ( $\sim 7$  MeV/nucleon). It was observed experimentally (stars) [6] that the charge distribution of both systems is almost identical, whereas their fragment multiplicities (IMFs) scale with the total charge of the colliding systems (4.4 in the case of  $^{129}\text{Xe} + ^{119}\text{Sn}$  and 6.4 in the case of  $^{155}\text{Gd} + ^{238}\text{U}$ ).

In the first place, Rivet *et al.* [31] and Frankland *et al.* [6] made efforts to reproduce these experimental observations by solving Boltzmann–Nordheim–Vlasov (BNV) equation in the initial steps, then performing simulations by using the stochastic initialization method (SIM) (by Rivet *et al.* [31]) and Brownian one-body dynamics (BOB) (by Frankland *et al.* [6]) calculations to determine intermediate times of the reaction. In both of these calculations, fragments were obtained by employing the minimum density cut and were realized at the time when multiplicity of various fragments saturates. In SIM calculations, the correct density fluctuations were added to the system when it enters into instability region, but afterward

standard one-body calculations were performed due to the lack of source term. On the other hand, in the case of BOB calculations, the density fluctuations were continuously acting due to the addition of a stochastic force term to the mean field. Therefore, the BOB calculations were considered more advanced than the SIM calculations. The fragments obtained from these models were excited; therefore, the deexcitation code SIMON (approximately after 200 fm/c) [32] was used to obtain realistic fragment structures. One should understand that the sources of different excitation energy and density produce a similar density distribution, although the system having smaller Coulomb barriers for fragment formation requires smaller temperature to break into fragments. They observed that SIM + SIMON (dashed double-dotted histograms) calculations deviate in reproducing the experimentally observed yield of the fragments with  $Z_f = 5, 6$  and  $Z_f > 25$ , whereas no such discrepancy was observed in case of BOB + SIMON calculations (dashed-dotted histograms). It should also be noted that in both cases of SIM or BOB + SIMON to make theoretical studies compatible with the experimental observations, the velocity component was added to fragments, lowering the excitation energy of the fragments. In the present calculations, QMD + SACA (open squares) not only reproduces the experimental trends but also the absolute values of the charge yields of all fragments. The observation time for  $^{129}\text{Xe} + ^{119}\text{Sn}$  and  $^{155}\text{Gd} + ^{238}\text{U}$  reactions depends on the rate of expansion of the nuclear matter; in the present study it is taken as 60 fm/c and 90 fm/c, respectively. The bottleneck in the QMD + SACA results is that one can realize the fragment configuration at the times when the nucleonic system is still in a highly nonequilibrium phase (or compressional phase) of the reaction. Note that even the fragments that are realized in compressional phase are not excited but are in their respective ground states.

Furthermore, in Fig. 2, we display the non-normalized charge distribution for the central reactions of  $^{129}\text{Xe} + ^{119}\text{Sn}$  and  $^{155}\text{Gd} + ^{238}\text{U}$  at incident energies of 32 and 36 MeV/nucleon, respectively. The solid lines in the figure represent the experimental observations. In earlier attempts to explain this experimental data, Raduta *et al.* [33] used the microcanonical multifragmentation model (MMM) to follow the initial phase of the reaction. At later times of the reaction, identified fragments were deexcited (approximately after 500 fm/c) by using the Weisskopf evaporation scheme [34]. They did employ two extreme freeze-out scenarios. In one case, fragments were considered as hard spheres placed into a spherical freeze-out recipient and the fragments were not allowed to overlap with each other as well as with the *receptacle* wall (hereafter called calculation 1) [13]. In other case, no hard-core interactions were considered (hereafter called calculation 2) [33]. The corresponding results of calculations 1 and 2 are denoted by crossed triangles and crossed circles, respectively. The MMM calculations with both these freeze-out conditions were able to reproduce the experimental data consistently [33]. The results of present calculations remain same as discussed earlier. Here again, QMD + SACA is able to reproduce the experimental results reasonably well.

It should be noted that, in the present calculations, the system evolves from the initial to the final state of the reaction with the effect of mean-field and collision terms; thus, no

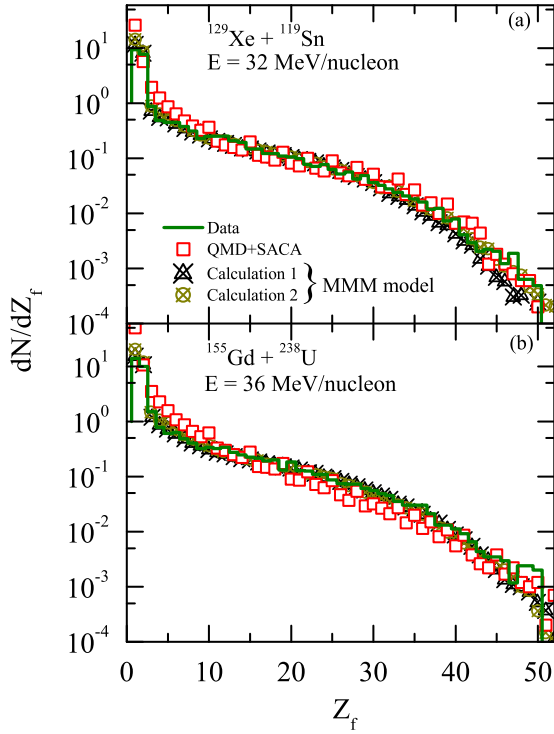


FIG. 2. The charge distribution obtained in the central reactions of  $^{129}\text{Xe} + ^{119}\text{Sn}$  and  $^{155}\text{Gd} + ^{238}\text{U}$  at an incident energy of 32 and 36 MeV/nucleon, respectively. The solid histograms represent experiment data [33] and the squares represent the calculations of QMD coupled with the SACA algorithm. The results of previous attempts [33] are also displayed for comparison.

equilibrium hypothesis is considered, as was assumed in other model calculations [6,31–33]. With the SACA method, we are able to reproduce the experimental charge distribution to all orders of magnitude. Also, no free parameters are used in the present analysis as were taken in all other model calculations to explain the experimental observations [33]. Moreover, the striking point of the QMD + SACA method is the faster realization of the fragment structures compared with all other previously used model results. Therefore, this method can shed light on the earlier dynamics of the fragment formation. Motivated by these results, let us see in the following the compatibility of QMD + SACA to explain some more complex observables used in the literature to study fragment properties [6].

In Fig. 3, we present the probability distribution of the first three largest charges emitted in the reactions of  $^{129}\text{Xe} + ^{119}\text{Sn}$  and  $^{155}\text{Gd} + ^{238}\text{U}$  at incident energies of 32 and 36 MeV/nucleon, respectively. The comparison of the probability distribution of the first three largest charges with the experimental observations allows us to check the reproduction of the event-by-event charge partition. If one compares the probability distribution of the largest charge, it can be inferred that the  $Z_f > 25$  region in the total charge distribution (see Fig. 2) is dominated by the first largest charge only. The results of BOB + SIMON [6] and MMM [33] calculations are also shown for comparative study. Symbols carry same meaning as in Fig. 2. It was observed that all these models reproduce the experimental data reasonably well. When we compare

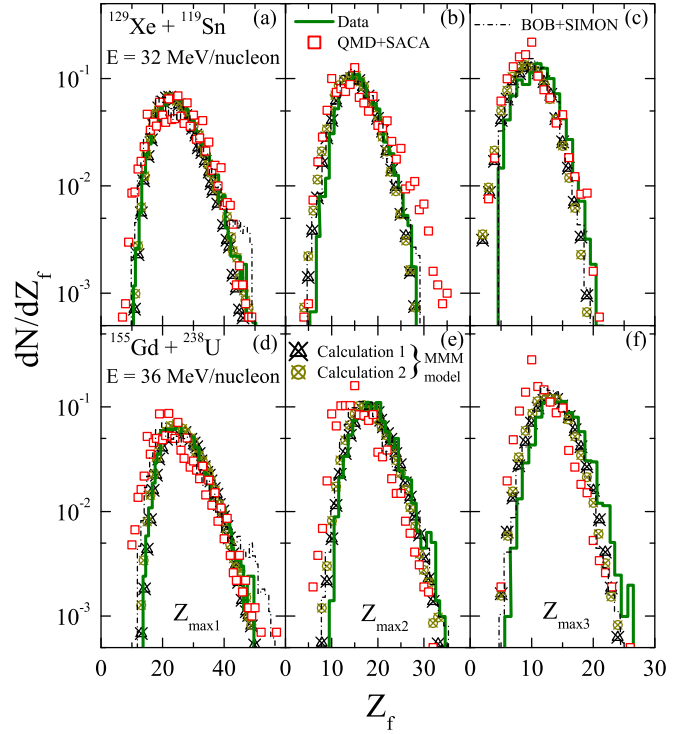


FIG. 3. The probability distribution of the *first three largest charges* emitted in central reactions of  $^{129}\text{Xe} + ^{119}\text{Sn}$  (top panels) and  $^{155}\text{Gd} + ^{238}\text{U}$  (bottom panels) at incident energies of 32 and 36 MeV/nucleon, respectively. Crossed triangles and crossed circles represent, respectively, the results of calculations 1 and 2 within the framework of the MMM model [33]. Other symbols have the same meaning as in Fig. 2.

our present calculations with experimental observations, we see that QMD + SACA consistently explains the experimental data of the probability distribution of the first, second, and third largest charges. The increasing difference between the average charges for the two reactions when going from the first to the second and the third largest charges is also well accounted for by the QMD + SACA calculations. This reflects the adequate description of the event charge distribution for the first three largest charges within each event. By observing these results, in the following we present results of event-by-event analysis of other observables.

In Fig. 4 (left panels), we display the probability distribution of the multiplicities of the IMFs [ $Z_f \geq 5$ ] for the central reactions of  $^{129}\text{Xe} + ^{119}\text{Sn}$  (top-left panels) and  $^{155}\text{Gd} + ^{238}\text{U}$  (bottom-left panel) at incident energies of 32 and 36 MeV/nucleon, respectively. In the right panel is the probability distribution of the total charge emitted as bound IMFs [bound IMFs ( $Z_{\text{bound}}$ ) in the present case is the sum of all fragment charges with  $Z_f \geq 5$ ] for the  $^{155}\text{Gd} + ^{238}\text{U}$  reactions. We also show the results of earlier attempts, i.e., SIM + SIMON [31] (dash double-dotted histograms), BOB + SIMON [6] (dash-dotted histograms), MMM [33] calculations (calculations 1 and 2 are represented by crossed triangles and crossed circles, respectively) for comparison. Note that, in case of the  $Z_{\text{bound}}$  distribution, results are not available with the SIM + SIMON

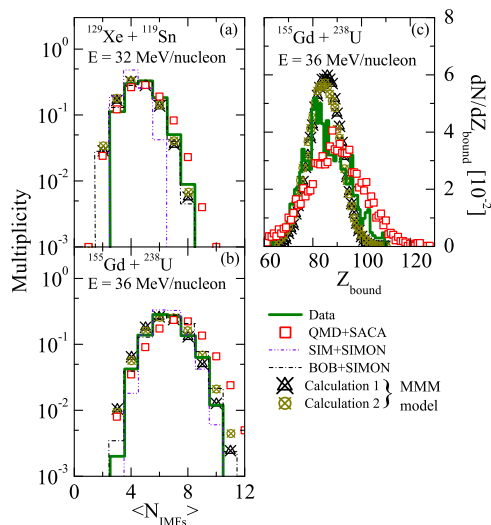


FIG. 4. Probability distribution of multiplicities of IMFs emitted in central reactions of  $^{129}\text{Xe} + ^{119}\text{Sn}$  (top-left panels) and  $^{155}\text{Gd} + ^{238}\text{U}$  (bottom-left panel) at incident energies of 32 and 36 MeV/nucleon, respectively [13,33]. In the right panel is the probability distribution of the charge of the IMFs emitted as bound fragments for the reactions of  $^{155}\text{Gd} + ^{238}\text{U}$  at an incident energy of 36 MeV/nucleon. Symbols have the same meaning as in Figs. 1 and 2.

and BOB + SIMON models. It can be observed from the figure that the SIM + SIMON (see dash double-dotted histograms) calculations show some discrepancy in reproducing the higher multiplicities for the reaction of  $^{129}\text{Xe} + ^{119}\text{Sn}$ . This inadequacy has been attributed to the lack of some kind of many-source dynamics in this model. The results become consistent when the BOB model was used in place of the SIM model. It was also observed that the results of MMM calculations, both for probability of multiplicities as well as  $Z_{\text{bound}}$  distribution, are consistent with the experimental observations, irrespective of the two different source parameters used in the calculations. Although, overprediction of the  $Z_{\text{bound}}$  peak was observed. In the present calculations, the QMD + SACA method is able to reproduce both the probability distribution of the multiplicities of IMFs as well as the probability distribution of the sum of charges of IMFs reasonably well. The slight overprediction in case of  $^{155}\text{Gd} + ^{238}\text{U}$  is due to the slight variation in the time chosen for final realization of the fragments. These results show the ability of SACA to identify fragment structures, irrespective of the fact that the nucleonic matter is still in a compressional phase. This happens because, in the SACA method, emphasis is on minimizing the system binding energy and not on checking the spatial separation between two nucleons. All the above results (from Figs. 1 to 4) are excellent examples governing the significance of the energy-based clusterization algorithm (SACA) to describe multifragmentation. These findings contribute to the solidity of the QMD + SACA approach to describe the fragmentation phenomena in the Fermi-energy domain.

Furthermore, with a thorough survey of the literature, we find that there exist other experimental results (e.g., for the

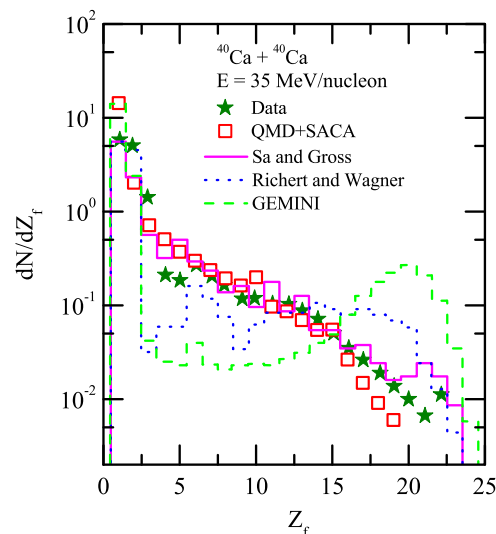


FIG. 5. The charge distribution obtained in the central reactions of  $^{40}\text{Ca} + ^{40}\text{Ca}$  at an incident energy of 35 MeV/nucleon. The stars represent the experimental data [35], and solid, dotted, and dashed histograms represent the calculations of Sa and Gross [36], Richert and Wagner [37], and GEMINI [24] models, respectively. The calculation obtained by using QMD coupled with SACA are represented by open squares.

central reactions of  $^{40}\text{Ca} + ^{40}\text{Ca}$  [35] and  $^{197}\text{Au} + ^{197}\text{Au}$  [7]) at nearly the same incident energy (35 MeV/nucleon). We shall, along with earlier-discussed results, also check the consistency of QMD + SACA results for these reactions. This gives us a unique opportunity to map the compatibility of QMD + SACA approach by keeping the excitation energy constant but varying the system mass as well as the mass asymmetry of colliding partners in the Fermi-energy domain. Also for these systems, theoretical calculations using statistical models are available in the literature, which will also help to produce a better picture of the fragmentation [7,35].

In Fig. 5, we show the fragment charge distribution for the central reaction of  $^{40}\text{Ca} + ^{40}\text{Ca}$  at an incident energy of 35 MeV/nucleon [35]. Hagel *et al.* [35] attempted to confront the experimental results for this reaction with various statistical calculations. To reproduce this fragment charge distribution, collisions were followed by using the Landau–Vlasov and BUU calculations until 70 fm/c and initial source conditions were estimated. Then, after estimating pre-equilibrium emission using Boltzmann master equation initial conditions of  $A_s = 70$ ,  $Z_s = 34$ , and  $E^* = 420$  MeV (here  $A_s$ ,  $Z_s$ , and  $E^*$  are mass, charge, and excitation energy of the source fragment) were determined and injected into statistical models of Sa and Gross (solid histograms) [36], Richert and Wagner (dotted histograms) [37], and GEMINI (dashed histograms) [24]. It is worth mentioning here that models of Sa and Gross, Richert and Wagner, and GEMINI are based on the simultaneous multifragmentation, sequential binary decay, and statistical decay calculations. They observed that the GEMINI model predicted a large production of  $Z_f = 1, 2$  and a very low production in the  $3 \leq Z_f \leq 15$  along with large value for heavy fragments. Compared to this, Richert and Wagner model calculations

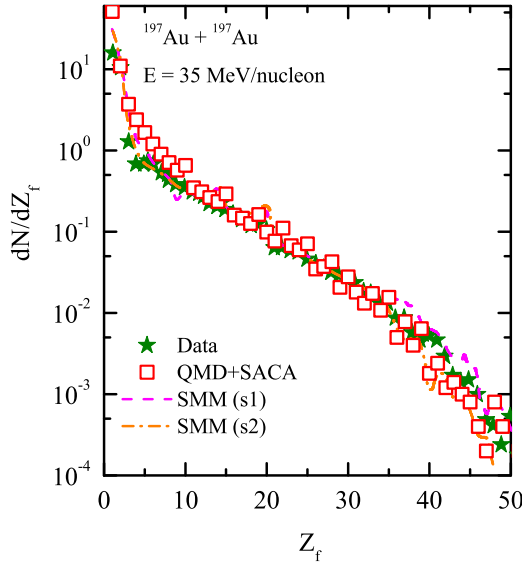


FIG. 6. The charge distribution obtained in the central reaction of  $^{197}\text{Au} + ^{197}\text{Au}$  at an incident energy of 35 MeV/nucleon. The stars represent the experimental data points extracted from Ref. [7]. The calculations obtained by using QMD + SACA are represented by open squares. The results of the statistical multifragmentation model (SMM) are also displayed for comparison [7].

gave a lesser value of heavy fragments and enhanced one in the intermediate charge bins. The experimental data were best described by the statistical multifragmentation code of Sa and Gross. In the present calculations, QMD + SACA, interestingly, reproduced the experimental data, suppressing the structural effect of magicity of colliding nuclei.

Next, in Fig. 6, we compare our calculations for the charge distribution of the central reactions of  $^{197}\text{Au} + ^{197}\text{Au}$  at an incident energy of 35 MeV/nucleon with experimental observations. For this system, it was observed that the radial kinetic energy of the fragments was small and thus, the assumption of equilibrium was not far from reality. Therefore, the statistical models could be checked for their compatibility. In this direction, Agostino *et al.* [7] used the SMM model with two source conditions to reproduce the experimental results. For simplicity, the different source conditions  $A_s = 343$ ,  $Z_s = 138$ ,  $E_s^* = 6.0$  MeV,  $\rho = \rho_0/3$  and  $A_s = 315$ ,  $Z_s = 126$ ,  $E_s^* = 4.8$  MeV,  $\rho = \rho_0/6$  (here  $A_s$ ,  $Z_s$ ,  $E_s^*$ , and  $\rho$  are mass, charge, excitation energy of the source fragment, and freeze-out density, respectively) are denoted by SMM (s1) and SMM (s2), respectively. The results of SMM (s1) and SMM (s2) are represented by dashed and dash-dotted lines, respectively. It was reported that both SMM (s1) and SMM (s2) were able to reproduce the experimental observations despite different source conditions. The results of the present calculations are repetitive of the earlier results, i.e., QMD + SACA reproduces the experimental charge distribution very nicely, although the slower expansion rate means that the fragments remain overlapped in coordinate space for longer durations. Therefore, the use of clusterization algorithms based on the spatial constraints cannot give realistic fragments. The other option is that one should wait for longer durations ( $\sim 1000$  fm/c) to let

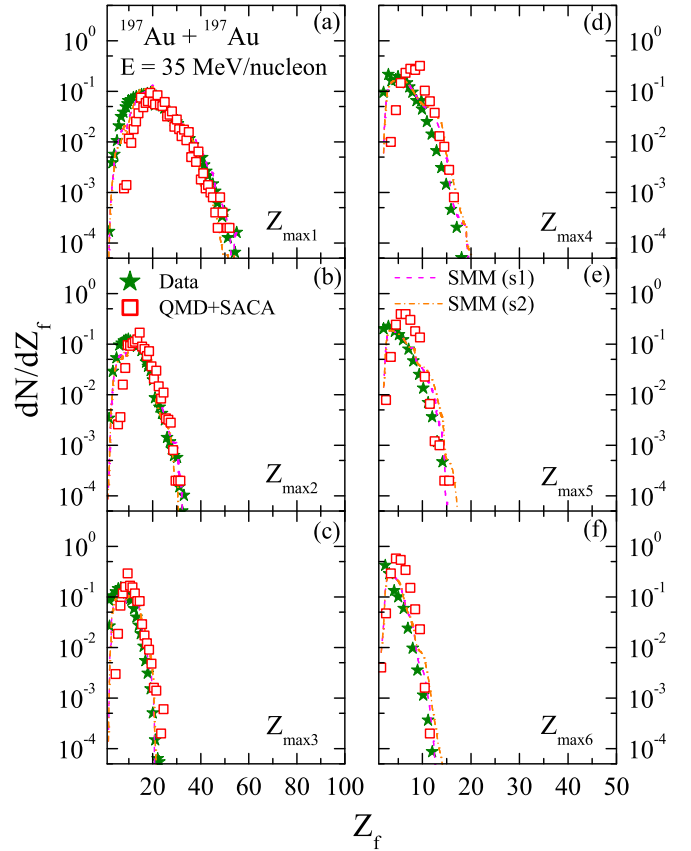


FIG. 7. Probability distribution of first six largest charges emitted in central reactions of  $^{197}\text{Au} + ^{197}\text{Au}$  at an incident energy of 35 MeV/nucleon [7]. Symbols have the same meaning as in Fig. 6.

the fragments separate out physically, which unfortunately is not allowed with molecular dynamics models (due to spurious emission of nucleons at later times). From the figure, we also see that QMD + SACA shows similar results as that observed previously by using the SMM model [7].

In Fig. 7, we present the charge partition within each event for the first six largest charges obtained in the central reactions of  $^{197}\text{Au} + ^{197}\text{Au}$  at an incident energy of 35 MeV/nucleon. Again, we see that the results obtained by using the QMD + SACA approach are the same as obtained earlier by using SMM model calculations. Note that the SMM [14] and QMD [12] models are based on entirely different assumptions. In the SMM model, the composite system is assumed to be in an equilibrated state; on the other hand, the QMD model follows the system according to the dynamical equations and collision terms. These are very surprising results, which make the question “is multifragmentation is statistical or dynamical?” more cumbersome.

Combining all these results and previously reported results in Refs. [27,29,30], it becomes clear that the QMD + SACA calculation reproduces experimental results very consistently over a wide range of entrance channels.

Finally, we feel that the calculated charge and probability distributions of first, second, third, fourth, fifth, and sixth largest charges, distribution of fragment multiplicities and

bound-charge distribution within each event presented here are very robust and thus the comparison with the experimental data remains fully meaningful. The overall agreement between experimental data and theoretical results using QMD + SACA is satisfactory in Fermi-energy domain. This study also shows the importance of the energy-based clusterization algorithm to describe fragmentation data. The same set of experimental data was also explained by using one-body as well as statistical approaches, but all these models identify the fragments only at later times, so they are less useful to explore the early dynamics of the reaction. Furthermore, as noted, one needs a heap of algorithms and models to explain a single experimental datum. On the other hand, with QMD + SACA one can find the fragment structures at early times, making it a powerful tool to study and explore the dynamics involved in the compressional phase of the reaction. Here as shown, just one model is enough and there is no need to apply a large number of models. Moreover, no assumption of any kind or fitting of parameters is made in SACA method to explain experimental data.

#### IV. SUMMARY

We have presented an exclusive comparison of the quantum molecular dynamics model coupled with the energy-based

clusterization algorithm, i.e., simulating annealing clusterization algorithm with experimental data in the Fermi-energy domain. Our results span over different system masses and system-mass asymmetries have been tested with the complex experimental data based on the event-by-event observables and not only with the global (average) observables. A detailed comparison of our calculations with one-body, statistical, and/or hybrid models was also made to get better picture of fragmentation. Our analysis shows that the energy-based clusterization algorithm coupled with the  $n$ -body dynamical model is more suitable to understand the dynamics involved in fragment formation because the fragments can be realized early, at times when the nucleonic matter is still in highly nonequilibrium conditions. Our calculations also rule out the need of a large number of models to explain single experimental observations.

#### ACKNOWLEDGMENT

This work is funded by Council of Scientific and Industrial Research (CSIR), Govt. of India, via Grant No. 03 (1388)/16/EMR-II.

- 
- [1] M. Begemann-Blaich *et al.*, *Phys. Rev. C* **48**, 610 (1993).  
 [2] A. Schüttauf *et al.*, *Nucl. Phys. A* **607**, 457 (1996).  
 [3] G. F. Peaslee, M. B. Tsang, C. Schwarz, M. J. Huang, W. S. Huang, W. C. Hsi, C. Williams, W. Bauer, D. R. Bowman, M. Chartier, J. Dinius, C. K. Gelbke, T. Glasmacher, D. O. Handzy, M. A. Lisa, W. G. Lynch, C. M. Mader, L. Phair, M. C. Lemaire, S. R. Souza, G. VanBuren, R. J. Charity, L. G. Sobotka, G. J. Kunde, U. Lynen, J. Pochodzalla, H. Sann, W. Trautmann, D. Fox, R. T. deSouza, G. Peilert, W. A. Friedman, and N. Carlin, *Phys. Rev. C* **49**, R2271(R) (1994).  
 [4] L. Phair *et al.*, *Nucl. Phys. A* **548**, 489 (1992).  
 [5] M. B. Tsang, W. C. Hsi, W. G. Lynch, D. R. Bowman, C. K. Gelbke, M. A. Lisa, G. F. Peaslee, G. J. Kunde, M. L. Begemann-Blaich, T. Hofmann, J. Hubele, J. Kempter, P. Kreuz, W. D. Kunze, V. Lindenstruth, U. Lynen, M. Mang, W. F. J. Muller, M. Neumann, B. Ocker, C. A. Ogilvie, J. Pochodzalla, F. Rosenberger, H. Sann, A. Schüttauf, V. Serfling, J. Stroth, W. Trautmann, A. Tucholski, A. Worner, E. Zude, B. Zwieglinski, S. Aiello, G. Imme, V. Pappalardo, G. Raciti, R. J. Charity, L. G. Sobotka, I. Iori, A. Moroni, R. Scardoni, A. Ferrero, W. Seidel, T. Blaich, L. Stuttge, A. Cosmo, W. A. Friedman, and G. Peilert, *Phys. Rev. Lett.* **71**, 1502 (1993).  
 [6] J. D. Frankland *et al.*, *Nucl. Phys. A* **689**, 940 (2001); J. D. Frankland, A. Chbihi, A. Mignon, M. L. Begemann-Blaich, R. Bittiger, B. Borderie, R. Bougault, J. L. Charvet, D. Cussol, R. Dayras, D. Durand, C. Escano-Rodriguez, E. Galichet, D. Guinet, P. Lantesse, A. Le Fevre, R. Legrain, N. LeNeindre, O. Lopez, J. Lukasik, U. Lynen, L. Manduci, J. Marie, W. F. J. Muller, L. Nalpas, H. Orth, M. Parlog, M. Pichon, M. F. Rivet, E. Rosato, R. Roy, A. Saija, C. Schwarz, C. Sfiinti, B. Tamain, W. Trautmann, A. Trzcinski, K. Turzo, A. VanLauwe, E. Vient, M. Vigilante, C. Volant, J. P. Wieleczko, and B. Zwieglinski (INDRA and ALADIN Collaborations), *Phys. Rev. C* **71**, 034607 (2005).  
 [7] M. D'Agostino *et al.*, *Phys. Lett. B* **371**, 175 (1996).  
 [8] G. F. Bertsch and S. D. Gupta, *Phys. Rep.* **160**, 189 (1988).  
 [9] H. Kruse, B. V. Jacak, and H. Stöcker, *Phys. Rev. Lett.* **54**, 289 (1985).  
 [10] C. Grégoire *et al.*, *Phys. Lett. B* **186**, 14 (1987).  
 [11] A. Badalá, R. Barbera, A. Bonasera, M. Di Toro, A. Palmeri, G. S. Pappalardo, F. Riggi, G. Russo, G. Bizard, D. Durand, and J. L. Laville, *Phys. Rev. C* **43**, 190 (1991).  
 [12] J. Aichelin, *Phys. Rep.* **202**, 233 (1991).  
 [13] Al. H. Raduta and Ad. R. Raduta, *Phys. Rev. C* **55**, 1344 (1997).  
 [14] J. P. Bondorf *et al.*, *Nucl. Phys. A* **444**, 460 (1985); A. S. Botvina *et al.*, *ibid.* **475**, 663 (1987).  
 [15] C. Hartnack *et al.*, *Eur. Phys. J. A* **1**, 151 (1998).  
 [16] E. Lehmann, R. K. Puri, A. Faessler, G. Batko, and S. W. Huang, *Phys. Rev. C* **51**, 2113 (1995).  
 [17] J. Singh and R. K. Puri, *Phys. Rev. C* **62**, 054602 (2000).  
 [18] S. Kumar and R. K. Puri, *Phys. Rev. C* **58**, 320 (1998); *J. Phys. G: Nucl. Part. Phys.* **27**, 2091 (2001).  
 [19] S. Kumar and R. K. Puri, *Phys. Rev. C* **58**, 2858 (1998).  
 [20] S. Goyal and R. K. Puri, *Phys. Rev. C* **83**, 047601 (2011).  
 [21] C. Ngo *et al.*, *Nucl. Phys. A* **499**, 148 (1989).  
 [22] R. Kumar, S. Gautam, and R. K. Puri, *Phys. Rev. C* **89**, 064608 (2014); *J. Phys. G: Nucl. Part. Phys.* **43**, 025104 (2016).  
 [23] K. Zbiri, A. Le Fevre, J. Aichelin, J. Lukasik, W. Reisdorf, F. Gulminelli, U. Lynen, W. F. J. Muller, H. Orth, C. Schwarz, C. Sfiinti, W. Trautmann, K. Turzo, B. Zwieglinski, J. L. Charvet, A. Chbihi, R. Dayras, D. Durand, J. D. Frankland, R. Legrain, N. LeNeindre, O. Lopez, L. Nalpas, M. Parlog, E. Plagnol, M. F. Rivet, E. Rosato, E. Vient, M. Vigilante, C. Volant, and J. P. Wieleczko, *Phys. Rev. C* **75**, 034612 (2007).  
 [24] R. J. Charity *et al.*, *Nucl. Phys. A* **483**, 371 (1988).  
 [25] W. Müller, M. Begemann-Blaich, and J. Aichelin, *Phys. Lett. B* **298**, 27 (1993).

- [26] C. O. Dorso and J. Randrup, *Phys. Lett. B* **301**, 328 (1993); C. O. Dorso and J. Aichelin, *ibid.* **345**, 197 (1995); P. N. Alcain and C. O. Dorso, *Phys. Rev. C* **97**, 015803 (2018).
- [27] R. K. Puri, C. Hartnack, and J. Aichelin, *Phys. Rev. C* **54**, R28 (1996); R. K. Puri and J. Aichelin, *J. Comput. Phys.* **162**, 245 (2000).
- [28] A. Le Fevre *et al.*, *J. Phys.: Conf. Ser.* **668**, 012021 (2016).
- [29] Y. K. Vermani *et al.*, *J. Phys. G: Nucl. Part. Phys.* **37**, 015105 (2010); S. Sood *et al.*, *Int. J. Pure Appl. Phys.* **13**, 201 (2017).
- [30] Y. K. Vermani and R. K. Puri, *Europhys. Lett.* **85**, 62001 (2009); S. Sood, I. Puri, R. Kumar, and R. K. Puri, *Int. J. Eng. Technol. Manag. Appl. Sci.* **5**, 2 (2017).
- [31] M. F. Rivet *et al.*, *Phys. Lett. B* **430**, 217 (1998).
- [32] A. D. N'guyen, Ph.D. thesis, Université de Caen, 1998 (unpublished).
- [33] A. H. Raduta and A. R. Raduta, *Phys. Rev. C* **65**, 054610 (2002).
- [34] A. H. Raduta and A. R. Raduta, *Phys. Rev. C* **61**, 034611 (2000).
- [35] K. Hagel, M. Gonin, R. Wada, J. B. Natowitz, B. H. Sa, Y. Lou, M. Gui, D. Utley, G. Nebbia, D. Fabris, G. Prete, J. Ruiz, D. Drain, B. Chambon, B. Cheynis, D. Guinet, X. C. Hu, A. Demeyer, C. Pastor, A. Giorni, A. Lleres, P. Stassi, J. B. Viano, and P. Gonthier, *Phys. Rev. Lett.* **68**, 2141 (1992).
- [36] S. Bam-Hao and D. H. E. Gross, *Nucl. Phys. A* **437**, 643 (1985); X.-Z. Zhang *et al.*, *ibid.* **461**, 641 (1987).
- [37] J. Richert and P. Wagner, *Nucl. Phys. A* **517**, 399 (1990).